Vacuum 219 (2024) 112701

Contents lists available at ScienceDirect

Vacuum

journal homepage: www.elsevier.com/locate/vacuum

Cylindrical hot cathode ionisation gauge – The concept and simulations

Ricardo A.S. Silva *, Nenad Bundaleski, Orlando M.D.N. Teodoro

CeFiTec, Department of Physics, Nova School of Science & Technology, Nova University Lisbon, 2829-515, Caparica, Portugal

ARTICLE INFO

Handling Editor: Prof. L.G. Hultman

Keywords:
Ionisation vacuum gauge
Accuracy
Simulation
SIMION

ABSTRACT

A novel design of an ionisation vacuum gauge is presented, aiming to achieve predictable sensitivity and high accuracy in high and the ultra-high vacuum range. The proposed design features a belt-like electron beam emitted from a linear filament, following a circular trajectory between two cylindrical electrodes, resembling a cylindrical analyser. The proposed design offers several key upsides: a precisely defined electron beam trajectory with reduced susceptibility to path variations, effective electron collection in a Faraday cup able to contain secondary emissions and backscattered electrons, and the inclusion of a suppressor grid in front of the ion collector to eliminate ion-induced secondary electron emission. These features are expected to secure high stability of the gauge and the low pressure limit. An in-depth description of the design is presented, along with the discussions on simulations of the key components that provide the improved performance.

1. Introduction

High and ultra-high vacuum (UHV) are essential in various fields of science, such as plasma physics, elementary particle physics, synchrotron radiation physics, gravitational wave detectors, and surface analysis. Moreover, vacuum in this range is also essential in some industrial applications, such as the production of thin films and semiconductor industry [1]. Despite advances in vacuum technology, accurately measuring pressure in this range remains challenging. Ionisation vacuum gauges are used for that purpose, but they suffer from limitations in accuracy and precision, which can lead to critical measurement errors in certain applications.

For instance, these gauges can exhibit deviations in sensitivity of tenths of a percent within 72 h, and a few percent within six months. Additionally, there can be a variation in sensitivity up to ±20% from one gauge to another of the same model [2–4]. Modern metrologically accurate gauges, such as the Stabil-Ion gauge, can exhibit stabilities on the order of 2% over 15 years under controlled conditions [5]. However, regular usage with exposure to various gases can lead to increased instability and decreased accuracy. Inaccuracies and lack of reproducibility in pressure measurements within the high and ultra-high vacuum range can have significant consequences, particularly in industrial settings. Such variations can impact the reliability of processes and lead to increased downtime and recalibration costs. In experimental science, accurate pressure measurements are critical for interpreting results and creating controlled environments. Therefore, a more stable gauge can reduce the frequency of recalibration and maintenance, improving the overall performance and reliability of a vacuum system.

Various attempts to measure pressure in this range using other phenomena besides ionisation have been made over the years. However, until the present moment, no other type of gauge has surpassed the simplicity and possibility of measuring such a wide pressure range as a hot cathode ionisation gauge. For instance, the spinning rotor gauge (SRG) [6], which partially covers the high vacuum range, is mainly used for metrological purposes. Its latest version enables highly accurate measurements from 5×10^{-7} mbar to 10^{-2} mbar (mainly above 10^{-5} mbar). The main reasons for its almost exclusive use in metrology are the need for a secondary instrument with lower pressure limit to establish its offset, the requirement for a controlled and vibration-free environment, and its non-continuous pressure measurement due to the long acquisition time necessary to increase signal to noise ratio. Recently, a new laboratory setup was developed by the National Institute of Standards and Technology (NIST) [7], as well as its miniature version [8], which allows for ultra-high vacuum measurement. In this new device, the laser cooling technique is used to create ultra-cold atoms (in the microkelvin range) that are magnetically confined in a small volume. The collision of atoms and molecules from the residual gas of the system is sufficient to decrease the population of confined atoms, and an exponential decrease in population occurs where the decay time constant is directly proportional to the system pressure. This setup is characterised by long acquisition times at low pressures (according to the authors, the device requires 100 s to measure a pressure of 1×10^{-10} mbar) similarly to the

* Corresponding author.
E-mail address: ras.silva@campus.fct.unl.pt (R.A.S. Silva).

https://doi.org/10.1016/j.vacuum.2023.112701
Received 1 August 2023; Received in revised form 12 October 2023; Accepted 13 October 2023
Available online 14 October 2023

drawbacks of SRG, making it highly impractical in the XHV range. Besides, this instrument is much more complex than any ionisation gauge and its main target is for metrological use.

In recent years, there has been an increasing trend towards utilizing simulations to comprehend the factors that affect the accuracy of ionisation gauges. They appear to be highly useful tools in that respect. Kauert and co-authors [9] took the initiative by conducting a three-dimensional simulation of a Stabil-Ion Gauge using a homemade program IONTRA3d that included, for the first time, the ionisation event. Due to the low ionisation probability resulting in a high number of simulated electrons per generated ion, the lowest simulated pressure was 10^{-3} mbar, which corresponds to the upper pressure limit of this type of gauges. Juda et al. [10], used the OPERA software to conduct simulations of electron and ion trajectories in a Bayard-Alpert gauge, including space charge effects for the first time. Through these simulations, they quantified the probability of ion collection and estimated the gauge's sensitivity. In line with these efforts, our research group developed a simulation tool that utilizes Lua scripts running in parallel with the SIMION software. This tool has been employed to successfully simulate conventional devices such as Bayard-Alpert and extractor gauges [11,12]. Moreover, a recently proposed ionisation gauge design, which appears to be highly suitable for metrological applications in the high vacuum range [13–15], was entirely built on the basis of such simulations. Other research groups have also focused on simulating these pressure gauges using SIMION software [16,17], as well as employing COMSOL Multiphysics [18,19], and even creating custom simulations [20,21].

Hot cathode ionisation gauges can experience various sources of instability during operation. Electron impact within the gauge leads to the production of X-rays, desorbed neutrals, ions, and secondary electrons. Similarly, ion impact also generates secondary electrons. To ensure accurate measurement of the ion current, it is crucial to address all these processes. Additionally, the operation of Bayard-Alpert like gauges may face challenges due to changes in electron path length caused by filament replacement or mechanical deformation of the grid. Addressing these issues is essential for improving the overall precision and reliability of the gauges.

Another extremely important parameter of ionisation vacuum gauges is their low pressure limit, often driving the development of new designs such as the extractor gauge [22], Helmer gauge [23], AXTRAN [24] or Watanabe's gauges (Ion spectroscopy [25] and Bent belt-beam [26] gauges). This limit is determined by various effects that influence the ion collector current, besides gas ionisation. Most of them are results of the emission of secondary particles induced by primary electrons: X-ray photons, backscattered electrons, desorbed ions. Additionally, thermal outgassing during the operation and electron stimulated desorption of neutrals may also contribute to the low pressure limit. However, in contrast to the previous contributions, the last two are inversely proportional to the overall pumping speed of the ionisation region. Therefore, a general strategy to reduce the low pressure limit consists of separating the ion collector from the impact points of primary electrons.

In 2017, a European project under the EMPIR program (project 16NRM05 'IONGAUGE') was launched with the aim of developing a new ionisation gauge that would provide measurements with an error of no more than 1%, in a pressure range from 10^{-8} to 10^{-4} mbar. The resulting design was proposed as a reference gauge to the International Organization for Standardization [13–15,27,28]. During the project, other designs were proposed, including a cylindrical belt-like beam concept [13]. The present work shows the progresses in the development of that concept.

A detailed simulation study was performed to refine the geometry and evaluate the potential sources of inaccuracy. In this paper, the evolution of the gauge's design to reduce the undesired phenomena during its operation is described. The simulations of its performance are also presented, as well as the comparison between the sensitivities predicted by the simulations and obtained in preliminary experimental tests.

2. Design concept

The initial goals for the design were three-fold: controlling secondary emission processes to improve accuracy of the ion current measurement, ensuring predictable sensitivity and reducing the low pressure limit. In this section, the evolution of the design will be described based on the known problems that compromise the achievement of these objectives.

The sensitivity serves as the primary parameter that characterizes hot cathode ionisation gauges, as it establishes the relation between the measured ion current and the pressure. It is defined by the following equation:

$$S = \frac{I_c - I_{c0}}{I_e \bullet (p - p_0)} \tag{1}$$

where I_c represents the ion current during operation, I_e the emitted electron current, and p the pressure in the ionisation volume. I_{c0} and p_0 represent the ion current at the residual gas pressure, respectively. In order to achieve high accuracy, it is necessary to ensure that the sensitivity is constant in the short and long term.

After introducing some approximations suitable for low pressures sensitivity can be expressed as [13]:

$$S = \frac{\langle \int_0^L \sigma(E)\, dl \rangle}{kT} \bullet P_{coll}. \tag{2}$$

In this expression, $\langle \int_0^L \sigma(E)\, dl \rangle$ represents the average of the integral of the ionisation cross-section along the electron trajectories (note that electron energy E changes along the trajectory, so does σ), where L denotes the total distance travelled by each electron. k is the Boltzmann constant; T and P_{coll} are the gas temperature and the probability of collecting ions created inside the gauge, respectively. If we consider that the electrons have a constant energy along their path, then we can simplify the previous expression:

$$S = \frac{\langle L \rangle \bullet \sigma}{kT} \bullet P_{coll}, \tag{3}$$

where $\langle L \rangle$ represents the electrons' mean path length and σ is the ionisation cross section for that electron energy. Thus, sensitivity varies linearly with the mean path length of electrons that ionise the gas. It becomes than obvious that ensuring a well-defined and stable L is essential for achieving high stability.

2.1. Securing low uncertainty of the electron path

Several studies have focused on the changes of sensitivity caused by the instability of electron trajectories in gauges where the trajectories are not well defined and predictable. Pittaway qualitatively investigated the influence of the relative position between the filament and the anode in Bayard-Alpert gauges, revealing a sensitivity change due to changes in electron trajectories [29]. Other authors confirmed the strong influence of relative positions and potentials of the electrodes (including the envelope) on the sensitivity of this type of gauge by altering electron trajectories [30,31]. In general, all gauges in which electrons make multiple passes through an anode consisting of a mesh are prone to large changes on their sensitivity due to the electron path length modifications.

A solution to this limitation is to replace the swarms of electrons with an electron beam performing a single electron pass along the ionisation volume, as in the case of the Klopfer gauge [32] and the recently proposed "ISO" gauge [13]. Both have a clear advantage of well-defined trajectories, and ISO gauge has also a point electron emitter, so that the electrons always have the same emission point. The use of a single pass electron beam also brings other advantages in controlling the effect

of secondary emissions from the collection of electrons, as it will be described below.

The major disadvantage of using single pass beams is the potential limitation of the emitted electron current due to the effects of space charge. Since these gauges work with low energy electrons (at most 300 eV), the space charge turns out to be the great limiting factor, not allowing the use of electron currents as high as in "swarm" gauges. In the case of the Klopfer gauge, a magnetic field of 0.1 T aligned with the electron trajectory is used to maintain the electron beam. However, the introduction of a magnetic field brings complexity and can affect other processes taking place in a vacuum chamber.

In the proposed design, electrons follow belt-shaped paths so that electrons have circular trajectories between two concentric cylindrical electrodes, as shown in Fig. 1a). The geometry is similar to that of a cylindrical energy analyser, which is why it will be addressed as 'cylindrical gauge'. In this gauge, the electric field is negligible along the axial coordinate and the electrons are emitted from a linear filament parallel to the axis. The linear cathode is supported inside a box-shaped electrode which has a similar function as a common Wehnelt electrode: it has a negative potential with respect to the cathode, so that electrons are directed towards the useful ionisation region. Inside the ionisation region, as in a cylindrical energy analyser, the electric potential is defined by the voltages of the outer and inner electrodes, V_{outer} and V_{inner}, respectively, with corresponding radii R_{outer} and R_{inner}. The cathode is biased to the appropriate voltage so that electrons are accelerated to the passing energy (E_k) defined by:

$$\frac{E_k}{e} = \frac{V_{outer} - V_{inner}}{2 \ln\left(\frac{R_{outer}}{R_{inner}}\right)} \tag{4}$$

The use of an extra electrode after the cathode at a voltage equal to the equipotential at $R_0 \approx (R_{outer} + R_{outer})/2$ was considered to better define the extraction voltage [33]. But the simulations described in the next sections showed that such an electrode is not essential for the beam formation and was, therefore, excluded.

Ions generated by the electron collision with the residual gas are accelerated radially towards the outer electrode. The ion collector is restricted to a small fraction of the electron trajectories, to be spatially separated from electron emission and collection regions. Only ions generated in front of the collector will contribute to the measured ion current. Although this ion loss reduces the potentially achievable sensitivity, it has an important advantage of placing the collector out of the lines of sight of electron emission and collection, which are the main sources of secondary emissions that may compromise the accurate ion current measurement.

A similar approach was applied in the Klopfer and ISO gauge. In this gauge, there is a first order focusing effect every 127° due to the electrical potential distribution that is inversely proportional to the radius [33]. This focusing keeps the beam with low spatial dispersion along the entire trajectory, without the need to use magnetic fields as in the Klopfer gauge.

Another major source of instability in electron trajectories is the change that occurs at cathodes over time. During operation, the work function of the cathode can be locally altered, causing a change in the distribution of electron emission points [34]. Contamination with impurities, reaction with non-inert gases, and evaporation of coatings in the case of coated cathodes, such as yttria-coated iridium emitters, are some of the mechanisms that cause the areas of greatest emission along the cathode to change over time. As in most gauges, trajectories are highly dependent on the exact position of the electron emission at the cathode, leading to drifts of the gauge sensitivity. This problem was solved in the ISO gauge by using a point electron emitter. In the cylindrical gauge, this dependence is suppressed since the cathode is parallel to the axis of revolution of electrons, and the length of the electron trajectory is independent of the emission zone along the cathode. In this way, even if the most probable zone of emission from the cathode shifts over time, the length of electron trajectories will not be affected.

At one end of the cylindrical envelope of the gauge, a cover must be placed to allow the gas flow from a vacuum chamber into the interior of the gauge. This cover should contain openings that are not too wide, to prevent leaks or significant changes in the trajectories of charged particles. At the same time, the vacuum conductance should be sufficient to ensure that the pumping caused by the ionisation of the gauge does not create a significant pressure difference from the interior to the exterior of the gauge, thereby avoiding systematic errors.

A potential disadvantage of using a single pass electron beam is the strong influence of stray magnetic fields on its operation. Since the electron beam is well defined, its deflection may compromise the desired transmission. This also happens in other concepts based on the electron beam, such as the ISO gauge, where fields of only 200 μT in certain directions are enough to completely compromise the gauge operation [13].

The two major changes made later in the design of Fig. 1a) are represented in b) and c) of the same figure. These modifications aimed to further reduce the effects of the two main sources of secondary emission – interaction of (1) electrons and (2) ions with the electrodes. Each of these modifications will be described in the following two sub-sections.

2.2. Suppressing effects of the electron induced secondary emissions

The main design strategies to avoid irradiation of the ion collector by X-rays generated by the impact of electrons in the gauges are to reduce the collector area (as in the Bayard-Alpert design [35]), and to place the ion collector outside the ionisation volume (as in the extractor gauge [22], Helmer gauge [23] or the Watanabe's gauges [25,26]). While the first solution is not sufficient for the pressures bellow the order of 10^{-10}

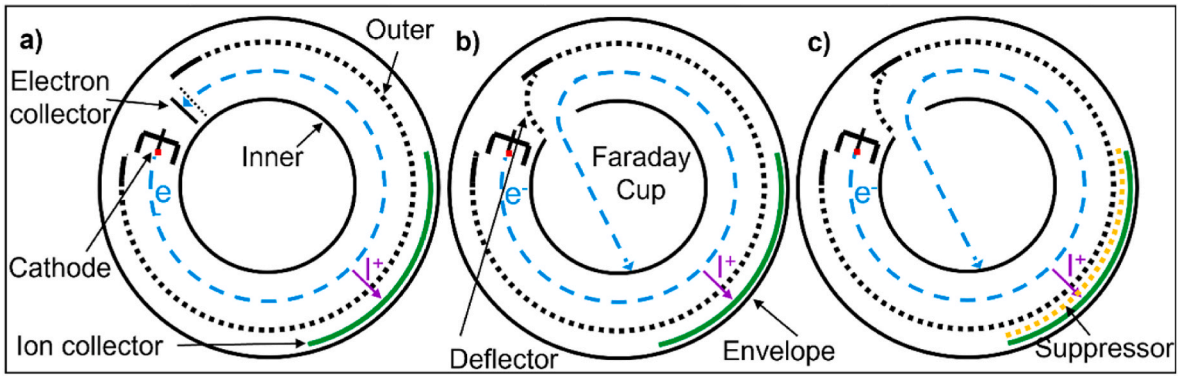

Fig. 1. Schematic representations of the evolution of the cylindrical gauge design: a) well-defined electron path; b) efficient electron collection; c) suppression of ion-induced secondary electron emission. The cathode is perpendicular to the drawing.

mbar, the second one has a drawback of a more complex design due to the necessity of ion extraction and, in some cases, reduction of P_{coll}. Besides, in the case of the extractor gauge, this method still does not tackle contribution of desorbed ions from the anode surface by the electron impact, which cannot be distinguished from the ions produced by electron impact ionisation of the gas. Other problems still exist in these gauges, such as the local increase of pressure due to the electron induced desorption of neutrals and particularly electron backscattering which prolongs their effective path length and can increase the sensitivity up to 10 % [12,36]. All these secondary particles would not compromise the stability of the sensitivity if their contribution to the sensitivity were constant at short and long term. However, except for X-rays, the yields of other secondary particles are strongly influenced by the composition of the first few atomic layers of the electrode responsible for electron collection, which changes during the operation [37].

To further improve the decoupling of ion current measurements from the secondary particles produced by electrons, the central electrode of the cylindrical gauge was opened on the opposite side of the ion collector to work as a Faraday cup, as shown in Fig. 1b). For this purpose, a new electrode is required to deflect the electrons into the Faraday cup, similarly to the solution applied in the ISO gauge [13]. This strategy is applicable namely because the primary electrons form a beam instead of a swarm. With this configuration, secondary electrons, desorbed ions, and X-rays should be effectively kept away from the ionisation region and from the ion collector. Therefore, they are not expected to change the measured ion current, as it will be demonstrated in the simulation section.

2.3. Avoiding ion induced secondary electron emission

The second modification consists of adding a suppressor grid in front of the ion collector with a negative potential to prevent the influence of secondary electron emission on the ion current measurement and photoelectrons (if some photons manage to reach the ion collector), as shown in Fig. 1c). This is a recurring solution to suppress the effect of secondary electron emission, applied in well-known gauges such as the Helmer gauge [23] or the ion spectroscopy gauge developed by Watanabe [38]. Although the introduction of a grid slightly reduces the sensitivity, because it is not fully transparent to ions, it appears to be a positive trade-off, as ion-induced secondary electron emission is one of the leading phenomena responsible for instabilities of ionisation gauges.

Not all gauges allow the addition of a suppressor electrode in front of the ion collector without significantly altering the particle trajectories, as is the case of Bayard-Alpert or ISO gauges. Therefore, in these gauges, it is recommended to perform a surface conditioning to the ion collector to stabilize the secondary electron emission. This procedure involves exposing the gauge to the upper pressure limit with an inert gas for a couple of hours. The use of a suppressor electrode in the cylindrical gauge better solves the same problem, saving time and preserving the filament lifetime.

3. Simulation

3.1. Simulation details

SIMION 8.1 was used to simulate and refine the geometry of the cylindrical gauge. Apart from its high reliability, this software was selected based on its capability to execute user-written scripts concurrently with the trajectories simulation. The scripts are algorithms written in the Lua programming language that were run in parallel to introduce additional features to the simulation (according to the Monte Carlo method), such as ionisation events and the backscattering of electrons in the Faraday cup [12].

The geometry of the electrodes was previously modelled in 3D using SolidWorks software (Fig. 2) and imported into SIMION as a CAD file in STL format. In all simulations, a resolution of 0.05 mm/gu and a convergence objective of 5×10^{-6} V were used. The electrons have initial energy of 0.1 eV and direction following a uniform hemispherical distribution. Table 1 shows the optimized voltages and principal dimensions of the gauge electrodes, obtained through an extensive simulation refinement process.

The simulation models used in this work were properly tested and described in previous works [12,14]. Briefly, to simulate the gas ionisation, the ionisation cross section is calculated at each step of the simulation as a function of the electron energy, through fittings of the cross sections calculated by the Binary-Encounter-Bethe (BEB) model [39]. Then, the ionisation probability is calculated and the ionisation events are modelled using the Monte Carlo method. Once an ion is created, its trajectory is followed. Since the probability of an electron causing ionisation is extremely low, each electron trajectory represents a

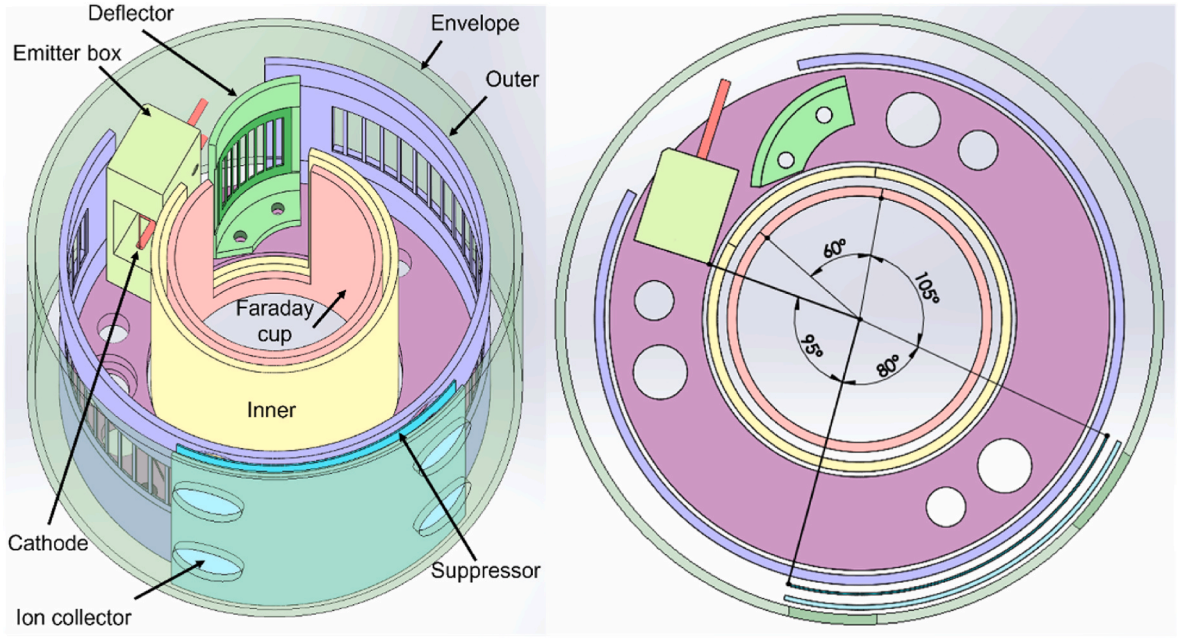

Fig. 2. 3D View of the cylindrical gauge; the upper cover is not represented to allow for observation of the inner electrodes as well as the assembling details.

Table 1
Voltages and main dimensions of the electrodes used in simulation.

Electrode	Voltage (V)	Length (mm)	Diameter/Radius (mm)
Cathode	10	12	Ø 0,15
Emitter box	−20	38x10x8	–
Outer	90	38	Ø 52
Inner	220	38	Ø 30
Deflector	−20	38	R11
Faraday cup	500	38	Ø 25
Suppressor	−15	38	R28
Ion collector	0	38	R29
Envelope	0	41	Ø 60

beam of N electrons. The value of N is calculated for each trajectory according to the criterion that the probability of this beam producing 0 or 1 ion is higher than 99% for the defined pressure and temperature. This makes the model valid only when the mean free path of the electrons is considerably greater than the average distance travelled by the electrons inside the gauge. Since this is also a criterion for the constant sensitivity of ionisation gauges, the model is applicable for the entire measurement range of these gauges. Electron backscattering is also simulated according to the Monte Carlo method. When a primary electron is collected on an electrode, the backscattering yield (BSY) is calculated based on the energy of impinging electrons and their incident angle with respect to the normal to the surface using the physical model from Drouin et al. [40]. This rate is defined as the ratio between the number of backscattered electrons and the number of incident electrons. When an electron is collected, a random value between 0 and 1 is generated, and if it is less than BSY, then backscattering is considered to occur. This electron is assigned a new energy and random direction following known backscattering distributions for aluminium [41].

The trajectories of ions are tracked, and the ions that reach the collector electrode are counted. The sensitivity of the gauge is then calculated at the end of each simulation by the ratio of collected ions to the total number of electrons divided by the pressure.

3.2. Simulation of electron trajectories

The simulation of electron trajectories was performed without using the LUA script to generate ionisation events. Electrons were defined to be emitted according to a Gaussian spatial distribution centred at the filament's midpoint and a standard deviation of 1 mm (see Fig. 3a), and b)) to model non-uniform distribution of emitted electrons along the filament.

A simulation was set with the voltages of Table 1 for 20 000 electrons with the above conditions and all were collected by the Faraday cup. It was found that the zone of the greatest spatial dispersion of the beam is already within the Faraday cup where there is no longer any influence

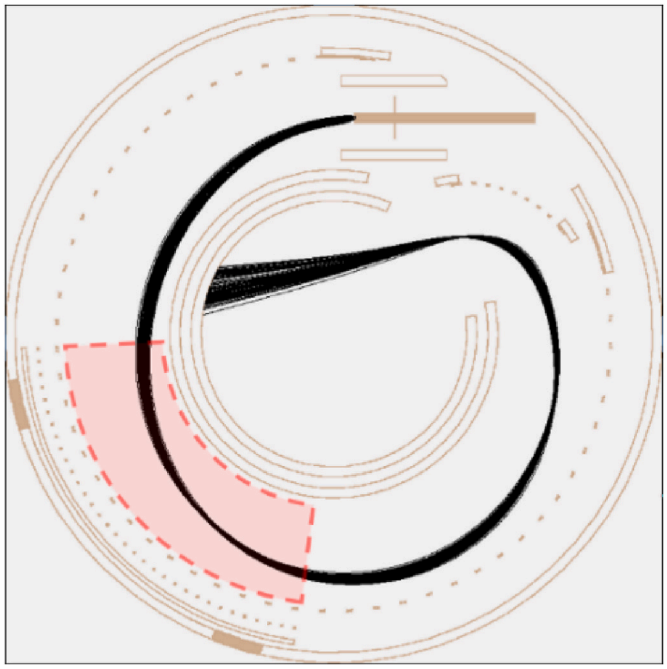

Fig. 4. Trajectories of the primary beam electrons; the red region represents the useful ionisation region, where the formed ions will impinge the ion collector and contribute to the measured ionic current.

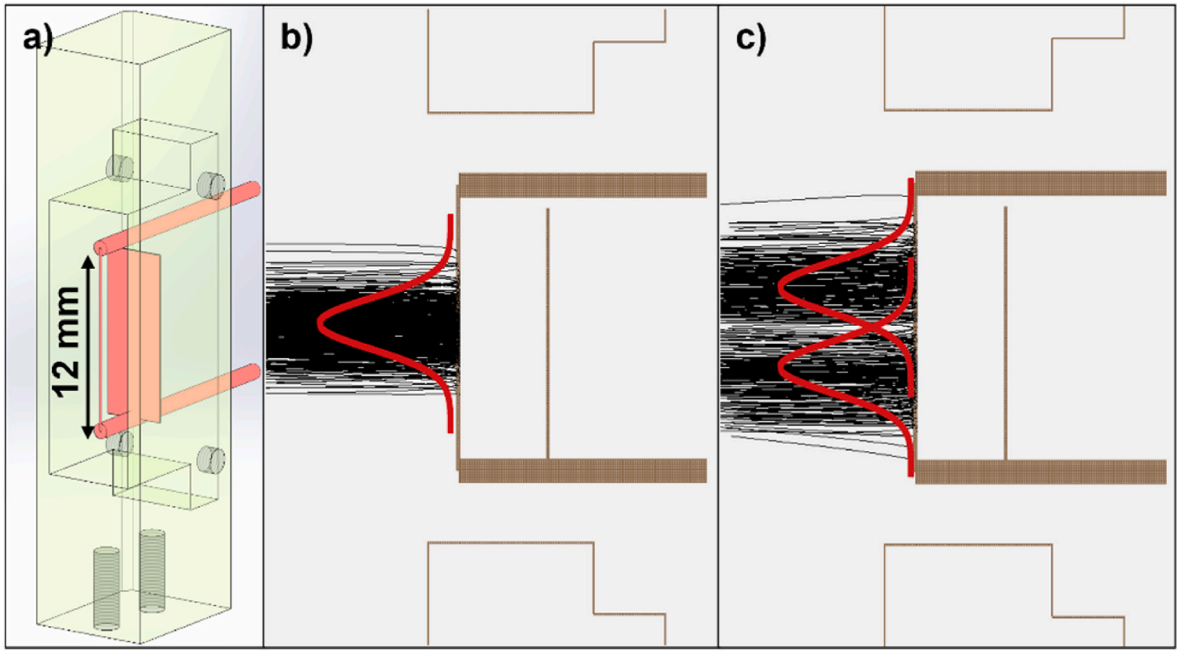

Fig. 3. Linear cathode in simulation: a) 3D perspective of the cathode and emitter box; b) regular simulated emission from the cathode; c) altered distribution of emission.

on the collection of ions (Fig. 4). As described in the design section, we can observe from the figure that there is a focusing effect due to the electric field between the inner and outer electrodes inversely proportional to the radius. The characteristic beam crossover points of cylindrical energy analysers can be clearly observed. However, the azimuth angles at which the crossover points occur do not correspond exactly to the theoretical angles ($\pi/\sqrt{2} \approx 127°$) of a cylindrical energy analyser [33] due to fringing fields in front of the cathode. Nevertheless, the focusing effect is highly advantageous in this application as it maintains the beam with low spatial and energy dispersion.

As described in the previous section, in order to achieve high stability and predictable sensitivity, the electrons' mean path length in the useful ionisation region must be well defined and constant in long term. This region is demarcated in red in Fig. 4. It represents the volume where the ions formed are directly attracted to the collector and contribute to the ion current. Through trajectory simulations, it was found that the mean path length in that region was 28.77 mm with a relative standard deviation of 0.4%. Fig. 5 shows the distribution of electrons' path length of 20 000 simulated electrons. Similar studies of trajectories inside a Bayard-Alpert type gauge reveal that trajectories are so disparate that the relative standard deviation of the path length is 88% [12].

In order to investigate the effect of the work function change along the filament during operation, a simulation was performed in which the initial conditions of the electrons were redefined. Electrons left the cathode following two Gaussian distributions shifted from the midpoint by +2 and −2 mm with a standard deviation of 1 mm as shown in Fig. 3c). It was found that the mean path length in the useful region was reduced only by 0.2%, proving that, in contrast to the most of the ionisation gauges working with swarms of electrons, a shift in the emission spot induced by a work function change would not lead to a noticeable change in the pressure reading. It was also found that filament misalignments less than 0.2 mm in the radial direction cause electron path length variations of less than 1%.

The ionisation cross section was calculated for different gases by fitting the cross sections calculated by the BEB model as a function of the electron energy along their trajectory (Fig. 6). It is found that during the passage of electrons in front of the ion collector, their kinetic energy increases because their radial coordinate decreases and so does their potential energy. The average energy of electrons in this interval is 138 eV, varying by about 70 eV along their path, corresponding to a variation of 51% relative to the mean value. However, this energy variation corresponds to the maximum variation of the ionisation cross section of only 12% for most gases. One should also have in mind that eventual lack of gauge stability is not related with the electron energy variation along the trajectory, but rather with the variations of trajectories (their lengths and the corresponding energies within the ionisation region) over the operation time of the gauge. Among the electrons in the beam,

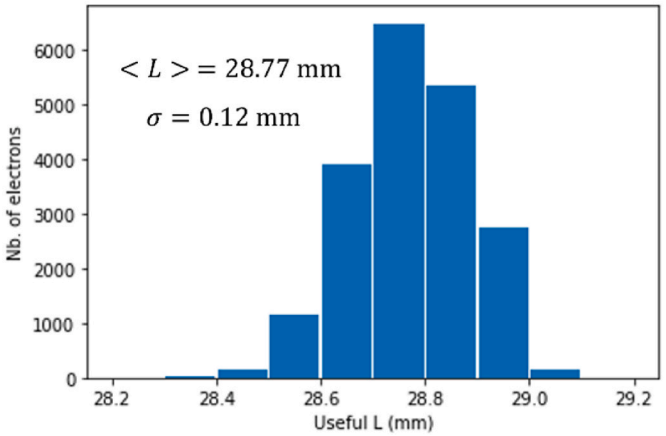

Fig. 5. Distribution of electron path length in the useful ionisation region.

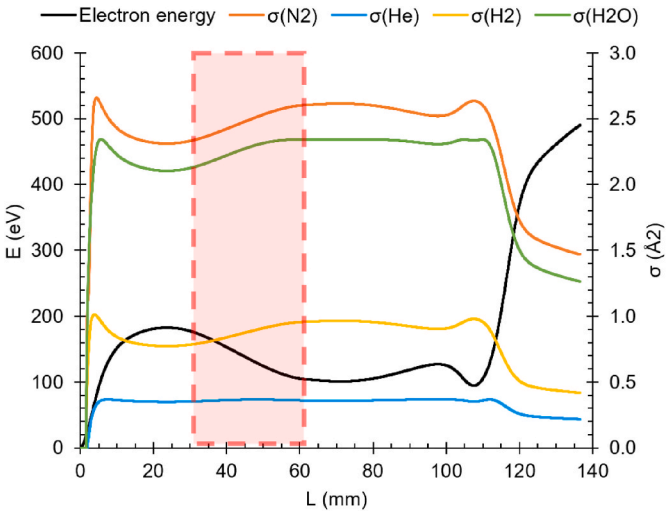

Fig. 6. Electron energy along its path and ionisation cross sections for different gases.

the integrated ionisation cross section along the trajectory has a standard deviation of only 0.55%, which reveals high coherence of the ionisation probability of electrons and confirms predictability of the gauge operation. In fact, this coherence of electron trajectories enables to predict in a straightforward manner expected sensitivity of this gauge operating with a specific gas, once the ionisation cross-section as a function of energy is known.

3.3. Modelling gas ionisation and predicting the sensitivity

As described earlier, when the simulation generates an ionisation event, the electron is transformed into an ion at the same point with a random initial velocity that follows the Maxwell distribution. The ions are then accelerated radially towards the outer electrode. Typical trajectories of electrons and ions inside the cylindrical gauge can be observed in Fig. 7. Only those ions formed in front of the ion collector contribute to the useful signal, while all others are collected by the envelope after passing the outer electrode. Since the collector azimuth angle covers 80° of the approximately 300°, the latter corresponding to the overall electron trajectory (cf. Fig. 2), only about ¼ of all ions are collected. The position and size of the collector electrode was chosen to provide absence of direct line of sight between this electrode and both the filament and the entrance into the Faraday cup. The azimuth angle of 80° is a trade-off, securing efficient decoupling of sources of secondary particles from the ion current measurement.

Simulations with different gases at different pressures were performed, allowing the calculation of sensitivity as a function of pressure. The sensitivity was found to be pressure independent, as expected, and its standard deviation is related to the statistical uncertainty inherent to the limited number of generated particles. To quantify the statistical uncertainty of the simulation, the same simulation was run several times with the same combination of parameters (pressure, temperature and number of particles), yielding in a relative sensitivity standard deviation of 1.2%. Fig. 8 plots the sensitivity as a function of pressure for nitrogen at 300 K. The mean sensitivity is 9.9 $mbar^{-1}$.

Table 2 summarizes the sensitivities determined for several gases at different temperatures. For each gas and temperature, 500 000 electrons were generated. Simulations were performed for three different temperatures since the true gas temperature inside ionisation gauges is unknown. It is certainly higher than the room temperature, since the cathode requires high temperature for thermionic emission, thereby heating the adjacent electrodes. Thus, the internal electrodes' temperature varies not only with the proximity to the filament, but is also considerably affected by the cathode design and type. It was confirmed

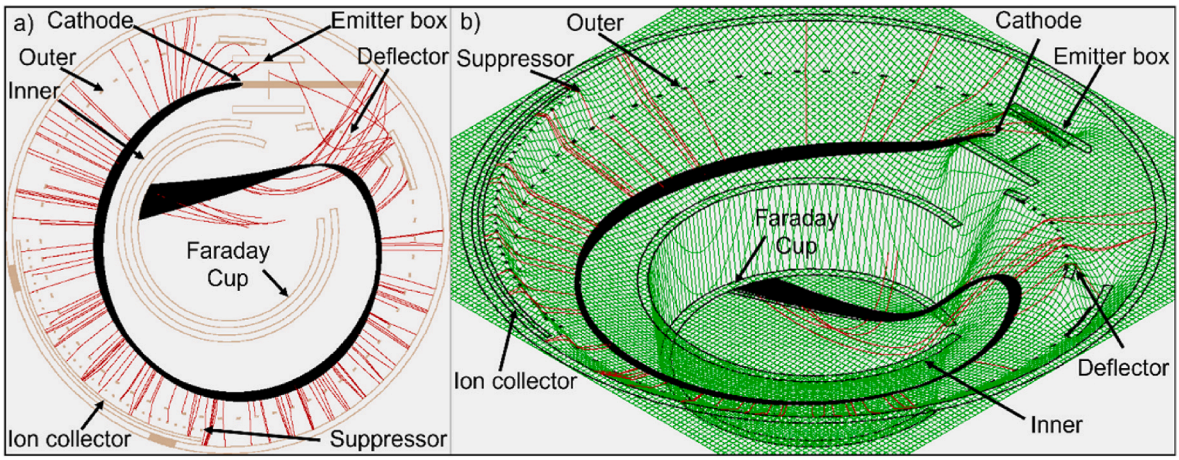

Fig. 7. SIMION simulation of electron (black lines) and ion (red lines) trajectories inside the gauge: a) regular representation after removing bottom and cover; b) electron potential energy surface representation corresponding to the mid plane of the gauge.

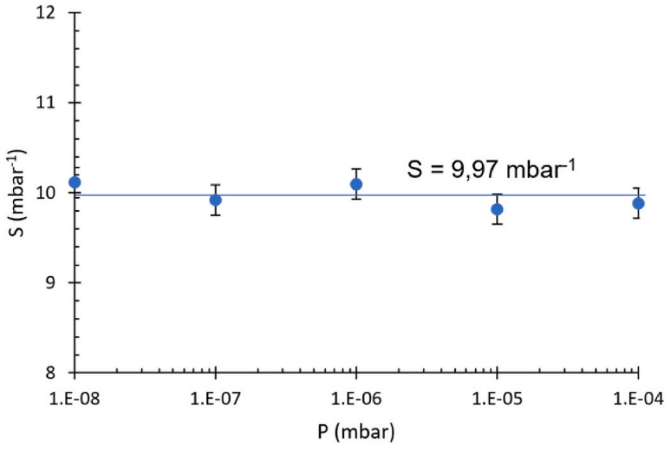

Fig. 8. Sensitivity as a function of pressure for nitrogen gas at 300 K.

that sensitivity is inversely proportional to temperature, as predicted by Equation (1).

The sensitivity predicted for this design is within the range of sensitivities common for hot cathode ionisation gauges. The sensitivity of the cylindrical gauge is slightly higher than that of an extractor gauge [42] but lower than most Bayard-Alpert gauge versions [10]. The higher the sensitivity, the higher will be the ion current for the same pressure and electron current. Sensitivity can be an issue only for low UHV when accuracy in measuring the ion current decreases. However, since the extractor gauge has sensitivity close to that of the cylindrical gauge such limitation should not be a problem to the same lower limit of 10^{-12} mbar.

The use of a belt like beam allows increasing its width without changing the trajectories. The simplest option is the use of a longer filament, but the use of multiple aligned cathodes is also acceptable. In this way, the electron beam current can be increased without compromising the gauge performance and facing the space charge problems. The outer electrode includes the top and bottom surfaces of the cylinder, generating a repelling field which confines the beam far enough from the tops avoiding any unwanted loss of electrons.

3.4. *Effect of the emitter box voltage on the transmission and sensitivity*

One of the main tuning parameters for the cylindrical gauge operation is the voltage of the emitter box, since it controls the dispersion of the electron beam. The more negative is its potential relative to the cathode, the lower is the electric field at the cathode surface due to a lower penetration of the external voltages. As a result, the emission area becomes more restricted, and the current is reduced. Widening of the electron beam in the radial direction is undesirable since the electron energy varies with the radius. In the extreme case, it is possible to start losing electrons due to collisions with electrodes, reducing the beam transmission (defined as the ratio between the current collected in the Faraday cup and the emitted current [13]) and generating secondary particles close to the ion collector. Hence, the voltage of the emitter box should be sufficiently negative to produce a narrow beam. Fig. 9 shows beams obtained with two different potentials applied to the emitter box, −20 and −10 V. When the potential is more repulsive for the electrons (−20 V), the beam obtained is notably narrower.

Fig. 10 shows the effect of varying the voltage of the emitter box on the sensitivity and the electron transmission. It was found that voltages below −15 V kept the beam sufficiently narrow and stable, while less repulsive voltages cause beam broadening affecting the transmission. It is relevant to emphasize that sensitivity obtained in the present simulation does not take into account the effects of secondary emission which may occur when the beam hits electrodes before entering the Faraday Cup. However, the simulation accounts for the effect of changing electron energies as they pass in front of the collector and electrons that are lost before passing in front of the ion collector.

3.5. *Secondary emission in the Faraday cup*

Simulations of primary electron trajectories revealed that it was possible to guide the entire beam into the Faraday cup. This raises the question of the efficiency of the Faraday cup design, which should ideally suppress the escape of secondary electrons, desorbed ions and

Table 2
Simulated sensitivities in $mbar^{-1}$ for each gas at different temperatures.

T (K)	N_2	He	H_2	Ar	H_2O	CO_2	CO	O_2	Ne	Kr	Xe
300	10.0	1.5	3.5	10.1	9.3	14.5	10.3	10.1	3.0	15.4	20.7
400	7.4	1.1	2.6	7.7	6.7	10.9	7.8	7.5	2.2	11.5	15.7
500	6.0	0.9	2.1	6.1	5.4	8.9	6.0	6.1	1.7	9.3	12.6

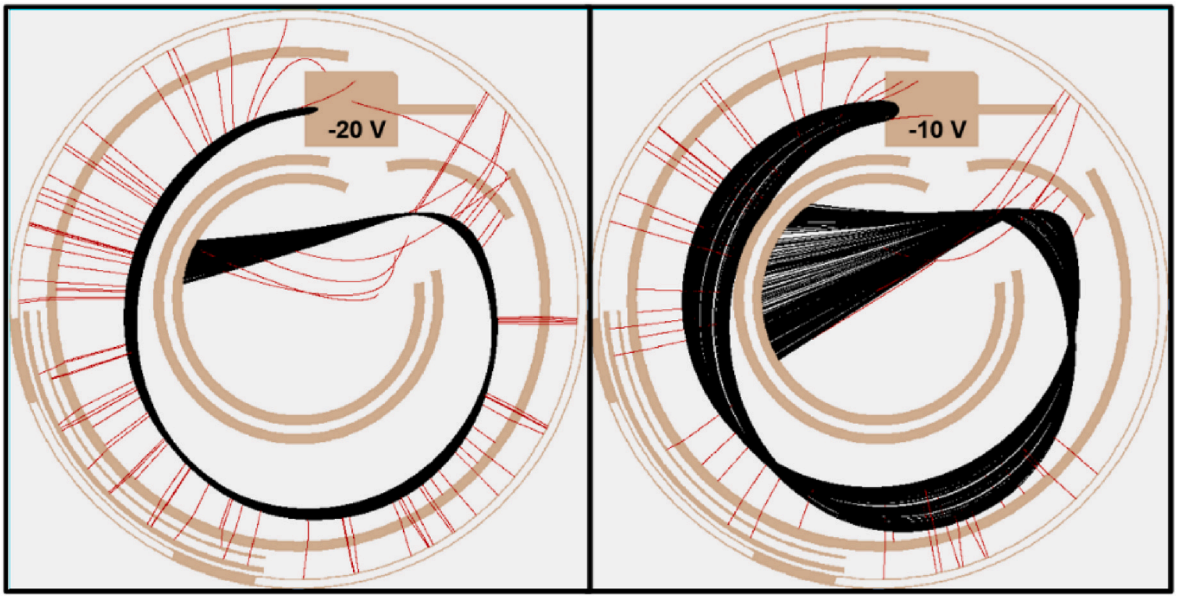

Fig. 9. Electron trajectories (black lines) when different potentials are applied to the Emitter box.

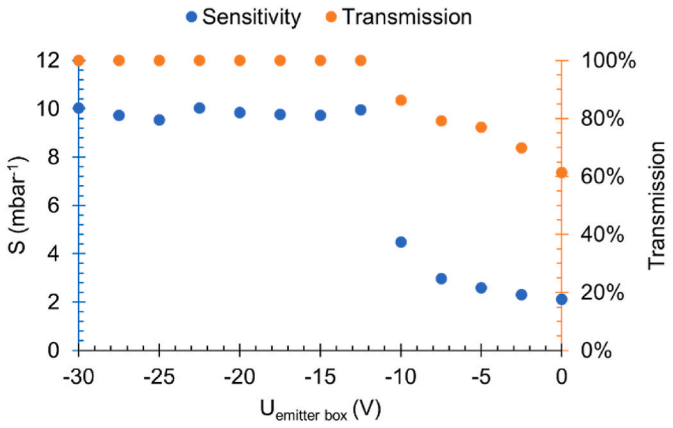

Fig. 10. Sensitivity and transmission as function of emitter box potential.

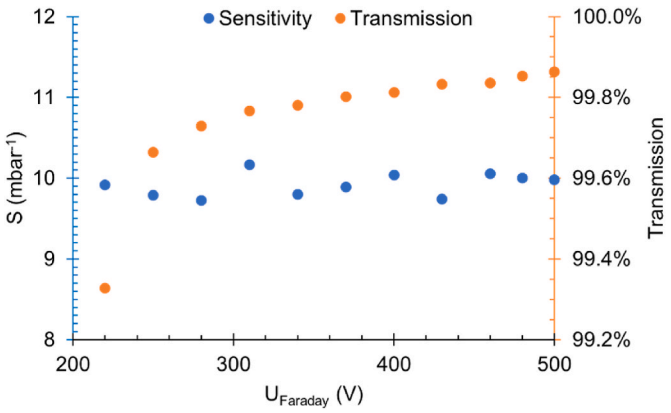

Fig. 11. Sensitivity and transmission as function of Faraday cup potential.

photons. When an electron collides with the electrode surface, backscattering or emission of secondary electrons may occur. True secondary electrons (considered to have energies below 50 eV [43]) are unlikely to escape the potential well created by the attractive Faraday cup. However, more energetic backscattered electrons might escape and eventually reach the useful ionisation region.

In an attempt to estimate the amount of electrons that are backscattered and escape the Faraday cup, simulations were performed with the inclusion of backscattering in the algorithm written in Lua (described in Section 3.1). Transmission in function of the Faraday cup voltage is presented in Fig. 11. It was found that by varying the potential between 220 and 500 V, the transmission is always greater than 99%, i.e. less than 1% of the backscattered electrons are able to escape the Faraday cup. However, in a more detailed simulation, it was found that the small uncollected fraction hits the inner electrode in a region close to the Faraday cup, as can be seen in Fig. 12. Even this small fraction of electrons should not affect the gauge operation since they are collected far away from the ion collector line of sight. Thus, sensitivity remains unchanged in simulations performed with and without the inclusion of the electron backscattering.

The geometry of the Faraday cup proved to be quite efficient in containing all types of secondary emission, as far as the simulations could show. This fact is evidenced by the low fraction of electrons that escape this electrode even when it is at the same potential as the inner electrode (220 V). In this configuration, the electrons are not in a potential well, yet only a small portion of electrons are not collected by the Faraday cup, due to the purely geometric confinement of this electrode. Simulations showed that some of the electrons are backscattered inside the Faraday cup more than once before being effectively collected. A similar phenomenon occurs with X-rays which have higher likelihood of colliding with the inner wall of the Faraday cup rather than passing through the cup's exit.

Desorbed ions are more likely to escape since the outer surface of the electrode is more attractive to them. However, the Faraday cup acts as a nearly field-free region, allowing only ions that pass near the exit to potentially leave. Even in these cases, these ions will be entirely collected by the deflecting electrode or the envelope, ensuring the proper functioning of the gauge and remaining far from the ion collector, as demonstrated in Fig. 12. Therefore, from the performed simulations, it is expected a high degree of Faraday cup efficiency in collecting all sorts of secondary particles. It is very unlikely that any significant amount of such particles could reach the ion collector and change the measurement of the intended ion current.

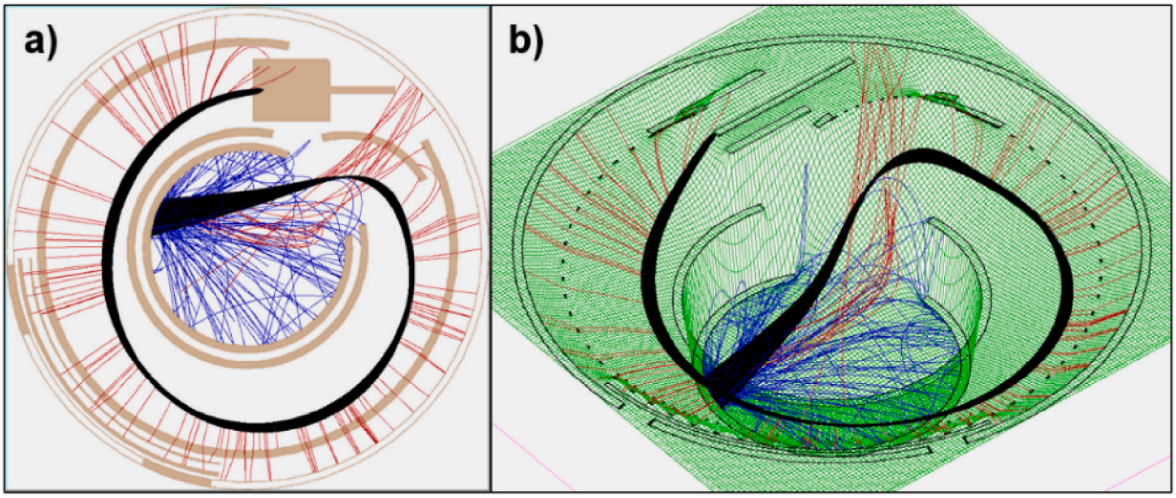

Fig. 12. Backscattered electron trajectories (blue lines) from the impinging primary electron beam (black lines) and ion trajectories (red lines): a) regular cut view from SIMION; b) electron potential energy surface view.

3.6. The suppressor grid

One of the most promising advantages of the cylindrical gauge design is the possibility of incorporating a suppression grid in front of the ion collector. This grid can eliminate the contribution of ion-induced secondary electrons at the ion collector. To test the efficiency of this grid in suppressing secondary emissions, electrons were emitted from the surface of the ion collector with different energies, with random initial velocities directed into the vacuum and uniformly distributed. The necessary energy of electrons to overcome the barrier and escape from the ion collector was determined as a function of the grid voltage (see Fig. 13). This figure shows that sensitivity remains constant regardless of the potential applied to the suppressor, which reveals that the transparency of the grid is not altered when varying its potential. This allows increasing the voltage until most of the secondary electrons are suppressed. Knowing that ions reach the surface of the collector with energies between 130 and 170 eV, for most gases the secondary electrons are emitted with energies lower than 15 eV [44]. Therefore, a potential of −30 V is sufficient to suppress such secondary electrons allowing an accurate ion current measurement.

The inclusion of the suppressor grid reduces the gauge sensitivity as it reduces the ion collection. The final design of the grid was 0.5 mm wide pillars and 2 mm spacing between them. According to simulations, the transparency of the suppressor grid is 74% which means that sensitivity is reduced by the same ratio when compared to the configuration without the grid. However, this is a beneficial trade-off since the emission of ion-induced secondary electrons is one of the important phenomena that contribute to drifts of the sensitivity. With the use of the suppressor electrode, the ion current is no longer dependent on the surface conditions of the collector, which is known to change during the gauge operation [37].

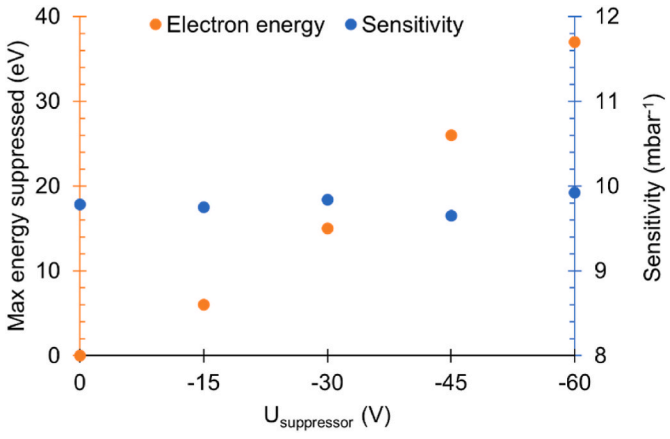

Fig. 13. Maximum energy of suppressed electrons and sensitivity as a function of the suppressor electrode potential.

3.7. Effect of magnetic fields

To investigate the influence of the magnetic field on the gauge's performance, electron trajectories were simulated under uniform magnetic fields throughout the entire gauge, overlapped with predefined electric fields. The direction and intensity of the magnetic field were varied, following a procedure similar to that described in Ref. [11]. By varying the field intensity from −10 to 10 Gauss in various directions, with a 0.2 Gauss interval, it was observed that for certain directions, a field strength of 1.4 Gauss was sufficient to partially compromise the transmission. For higher magnetic fields, a portion of the electron beam ceased to enter the Faraday cup. It was found that in the presence of magnetic fields exceeding 9.4 Gauss, regardless of their orientation, transmission became null, and the entire electron beam was collected by the other electrodes.

The simulation results suggest that this configuration will require magnetic shielding if it is necessary to operate in the vicinity of equipment that produces magnetic fields, such as cold cathode gauges or ion pumps.

3.8. Sensitivity prediction for each gas

In the preceding subsection, we computed the sensitivity for various gases by utilizing the Monte Carlo method to simulate ionisation. However, for practical purposes, it would be valuable to estimate the gauge's sensitivity to any arbitrary gas without resorting to simulation tools. This would allow users to assess the sensitivity of the gauge for a specific gas by considering only a few parameters and without a need for complex simulations. The key parameters required for this estimation are the ionisation cross-section ($\sigma_{g/138\ \mathrm{eV}}$) for the mean energy of electrons passing in front of the collector, the temperature (T), the electron path length in front of the collector (L = 28.7 mm), and the transparencies of the outer and suppressor grids (T_{outer} = 78.7% and $T_{suppressor}$ = 74.9%, respectively). By reformulating equation (3), we arrive at the following expression for calculating the gauge sensitivity (S_g) of a particular gas in units of mbar^{-1}:

$$S_g\left(\text{mbar}^{-1}\right) = 1.22502 \times 10^3 \frac{\sigma_{g/138\ \text{eV}}\left(\text{Å}^2\right)}{T(\text{K})} \quad (5)$$

To demonstrate the utility of this approach, we consider the ionisation cross-section for molecular nitrogen ($\sigma_{N_2}(138\ eV) = 2.526\ \text{Å}^2$) from the NIST database [45]. Assuming room temperature conditions ($T = 300$ K), the estimated sensitivity using equation (5) yields 10.31 mbar^{-1}. Importantly, this estimation displays a small relative error of 3% compared to the sensitivity obtained in the simulations, which takes into account electron energy variation along the path. Thus, equation (5) offers a simple and rapid method for predicting sensitivity of the cylindrical gauge for an arbitrary gas.

4. Preliminary experimental results

In order to establish the viability of our concept, we conducted preliminary experimental testing, as outlined in this section. To do this, we selected one of our prototypes and performed calibration using an MKS spinning rotor gauge 2. The cylindrical gauge was placed within a calibration chamber, and the system was subjected to a 48-h baking process at 150 °C. This initial calibration was carried out using Nitrogen gas (N2).

Fig. 14 displays the measured sensitivity in relation to pressure. It is noteworthy that the sensitivity remained consistent throughout the range of pressures tested, with an average sensitivity of 10.33 mbar-1 and a relative standard deviation of 0.6%. It is important to highlight that this experimental sensitivity value is approximately 4% higher than the value predicted by our simulation tools for the gas temperature of 300 K.

These results serve a dual purpose: they affirm the predictive accuracy of our simulation tools and demonstrate the functionality of the proposed design even in a reduced test pressure range. The publication of tests in a wider pressure range and with different gases is expected in the near future.

5. Conclusions and overview

A new concept of a hot cathode ionisation gauge with a cylindrical geometry was described with the aim of achieving high accuracy of pressure measurement in the HV and UHV range. The concept was tested and the geometric details of the design were refined on the basis of extended simulation work in SIMION. In the proposed design, a belt-like electron beam is emitted from a linear filament, describing a quasi-circular trajectory between two cylindrical electrodes, similar to a cylindrical analyser. Many details are discussed with the goal of decreasing the known sources of instability and low pressure limit. Simulations included ion and electron trajectories, ionisation events, backscattered electrons as well as electron and ion collection.

The main features of the proposed design are: (1) a belt-like electron beam with a well-defined path length and little susceptibility to changes; (2) the possibility of increasing the electron current by increasing the cathode length or by including multiple cathodes; (3) high efficiency in the collection of electrons in the Faraday cup which is able to contain secondary particles and backscattered electrons; (4) the possibility of including a suppressor grid in front of the ion collector that eliminates the effects of ion-induced secondary electron emission. These features increase the complexity of the design and require more electrodes then in Bayard-Alpert or extractor gauges.

In the present configuration, majority of documented sources of instability and low pressure limit were addressed. It is expected that this new design will offer greater accuracy compared to the traditional ionisation gauges. The outcomes of evaluation tests conducted on prototypes of the cylindrical gauge are anticipated to be published in the near future.

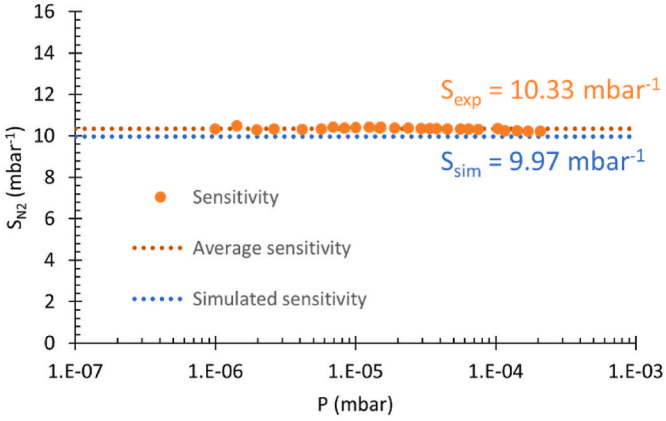

Fig. 14. Sensitivity calibration curve for N_2 and comparison with simulated sensitivity for T = 300 K.

CRediT authorship contribution statement

Ricardo A.S. Silva: Writing – review & editing, Writing – original draft, Methodology, Investigation, Formal analysis, Data curation, Conceptualization. **Nenad Bundaleski:** Writing – review & editing, Supervision, Methodology, Conceptualization. **Orlando M.D.N. Teodoro:** Writing – review & editing, Validation, Supervision, Project administration, Funding acquisition, Formal analysis, Conceptualization.

Declaration of competing interest

The authors declare that they have no known competing financial interests or personal relationships that could have appeared to influence the work reported in this paper.

Data availability

Data will be made available on request.

Acknowledgements

The support of the Portuguese Foundation for Science and Technology via the grants UIDB/00068/2020 and UIDP/00068/2020 is gratefully acknowledged. One of the authors (R.A.S. Silva) would like also to express his gratitude to the Portuguese Foundation for Science and Technology for his scholarship UI/BD/150626/2020.

References

[1] K. Jousten, Vacuum metrology and its impact on research and industry: from state of the art measurements to future trends, Vakuum Forsch. Praxis 31 (2019) 16–22, https://doi.org/10.1002/vipr.201900715.
[2] C.R. Tilford, Sensitivity of hot cathode ionization gages, J. Vac. Sci. Technol. A: Vacuum, Surfaces, and Films 3 (1985) 546–550, https://doi.org/10.1116/1.572991.
[3] D. Li, K. Jousten, Comparison of some metrological characteristics of hot and cold cathode ionisation gauges, Vacuum 70 (2003) 531–541, https://doi.org/10.1016/S0042-207X(02)00781-9.
[4] P.C. Arnold, S.C. Borichevsky, Nonstable behavior of widely used ionization gauges, J. Vac. Sci. Technol. A: Vacuum, Surfaces, and Films 12 (1994) 568–573, https://doi.org/10.1116/1.578835.
[5] J.A. Fedchak, D.R. Defibaugh, Long-term stability of metal-envelope enclosed Bayard–Alpert ionization gauges, J. Vac. Sci. Technol. A: Vacuum, Surfaces, and Films 30 (2012), https://doi.org/10.1116/1.4750482.
[6] J.K. Fremerey, The spinning rotor gauge, J. Vac. Sci. Technol. A: Vacuum, Surfaces, and Films 3 (1985) 1715–1720, https://doi.org/10.1116/1.573007.
[7] D.S. Barker, B.P. Acharya, J.A. Fedchak, N.N. Klimov, E.B. Norrgard, J. Scherschligt, E. Tiesinga, S.P. Eckel, Precise quantum measurement of vacuum with cold atoms, Rev. Sci. Instrum. 93 (2022), https://doi.org/10.1063/5.0120500.

[8] L.H. Ehinger, B.P. Acharya, D.S. Barker, J.A. Fedchak, J. Scherschligt, E. Tiesinga, S. Eckel, Comparison of two multiplexed portable cold-atom vacuum standards, AVS Quantum Science 4 (2022), 034403, https://doi.org/10.1116/5.0095011.
[9] R. Kauert, O.F. O Kieler, S. Biehl, W. Knapp, C. Edelmann, S. Wilfert, Numerical investigations of hot cathode ionization gauges, Vacuum 51 (1998) 53–59.
[10] P. Juda, B. Jenninger, P. Chiggiato, T. Richard, 3D-simulation of ionisation gauges and comparison with measurements, Vacuum 138 (2017) 173–177, https://doi.org/10.1016/j.vacuum.2016.12.014.
[11] R.A.S. Silva, N. Bundaleski, O.M.N.D. Teodoro, Effect of the magnetic field on the operation of ionisation gauges, Vacuum 204 (2022), https://doi.org/10.1016/j.vacuum.2022.111339.
[12] R. Silva, N. Bundaleski, A.L. Fonseca, O.M.N.D. Teodoro, 3D-Simulation of a Bayard Alpert ionisation gauge using SIMION program, Vacuum 164 (2019) 300–307, https://doi.org/10.1016/j.vacuum.2019.03.039.
[13] B. Jenninger, J. Anderson, M. Bernien, N. Bundaleski, H. Dimitrova, M. Granovskij, C. Illgen, J. Setina, K. Jousten, P. Kucharski, C. Reinhardt, F. Scuderi, R.A.S. Silva, A. Stöltzel, O.M.N.D. Teodoro, B. Trzpil-Jurgielewicz, M. Wüest, Development of a design for an ionisation vacuum gauge suitable as a reference standard, Vacuum 183 (2021), https://doi.org/10.1016/j.vacuum.2020.109884.
[14] N. Bundaleski, C.F. Adame, M. Bernien, C. Illgen, B. Jenninger, K. Jousten, F. Scuderi, R.A.S. Silva, A. Stöltzel, J. Šetina, O.M.N.D. Teodoro, T. Verbovšek, M. Vičar, M. Wüest, Novel ionisation vacuum gauge suitable as a reference standard: influence of primary electron trajectories on the operation, Vacuum 201 (2022), https://doi.org/10.1016/j.vacuum.2022.111041.
[15] K. Jousten, S. Bechstein, M. Bernien, F. Boineau, N. Bundaleski, C. Illgen, B. Jenninger, J. Šetina, R.A.S. Silva, A. Stöltzel, O.M.N.D. Teodoro, M. Wüest, Evaluation and metrological performance of a novel ionisation vacuum gauge suitable as reference standard, Measurement 210 (2023), https://doi.org/10.1016/j.measurement.2023.112552.
[16] J. Zhang, J. Wei, D. Li, H. Zhang, Y. Wang, X. Zhang, A cylindrical triode ultrahigh vacuum ionization gauge with a carbon nanotube cathode, Nanomaterials 11 (2021), https://doi.org/10.3390/nano11071636.
[17] X. Yuhuaf, L. Detian, W. Yongjun, Z. Huzhong, C. Yongjun, L. Danming, W. Shifa, Investigation of a spherical oscillator ionization gauges with carbon nanotube field-emitter cathodes, in: 2017 30th International Vacuum Nanoelectronics Conference (IVNC), 2017, pp. 182–183, https://doi.org/10.1109/IVNC.2017.8051600.
[18] S. Mohammadzadeh Bazarchi, E. Abaspour Sani, Simulation of bayard alpert ionization vacuum gauge with COMSOL, in: S. Montaser Kouhsari (Ed.), Fundamental Research in Electrical Engineering, Springer Singapore, Singapore, 2019, pp. 347–357.
[19] G. Wang, M. Yi, C. Chen, Z. Zhou, J. Wang, Y. Lin, Numerical simulation of the performance of the ASDEX pressure gauge, Vacuum 189 (2021), https://doi.org/10.1016/j.vacuum.2021.110237.
[20] S. Suginuma, Numerical simulation of relative sensitivity factor of Bayard–Alpert gauge, Vacuum 179 (2020), https://doi.org/10.1016/j.vacuum.2020.109525.
[21] A. Tegerup, Simulationof a Bayard-Alpert Ionization Gauge with the PIC Code Warp, KTH, Numerical Analysis, NA, 2018.
[22] P.A. Redhead, New hot-filament ionization gauge with low residual current, J. Vac. Sci. Technol. 3 (1966) 173–180, https://doi.org/10.1116/1.1492470.
[23] J.C. Helmer, W.H. Hayward, Ion gauge for vacuum pressure measurements below 1×10−10 torr, Rev. Sci. Instrum. 37 (1966) 1652–1654.
[24] N. Takahashi, J. Yuyama, Y. Tuzi, H. Akimichi, I. Arakawa, Axial-symmetric transmission gauge: extension of its pressure measuring range and reduction of the electron stimulated desorption ion effect in ultrahigh vacuum, J. Vac. Sci. Technol. A: Vacuum, Surfaces, and Films 23 (2005) 554–558, https://doi.org/10.1116/1.1901668.
[25] F. Watanabe, Ion spectroscopy gauge: total pressure measurements down to 10 −12 Pa with discrimination against electron-stimulated-desorption ions, J. Vac. Sci. Technol. A: Vacuum, Surfaces, and Films 10 (1992) 3333–3339, https://doi.org/10.1116/1.577821.
[26] F. Watanabe, Bent belt-beam gauge: extending low-pressure measurement limits in a hot-cathode ionization vacuum gauge by combining multiple methods, J. Vac. Sci. Technol. A: Vacuum, Surfaces, and Films 28 (2010) 486–494, https://doi.org/10.1116/1.3400233.
[27] K. Jousten, M. Bernien, F. Boineau, N. Bundaleski, C. Illgen, B. Jenninger, G. Jönsson, J. Šetina, O.M.N.D. Teodoro, M. Vičar, Electrons on a straight path: a novel ionisation vacuum gauge suitable as reference standard, Vacuum 189 (2021), https://doi.org/10.1016/j.vacuum.2021.110239.
[28] M. Bernien, M. Götz, C. Illgen, D. Drung, C. Krause, T. Bock, K. Jousten, Traceable low-current measurements for a novel ionization gauge suitable as reference standard, in: Measurement: Sensors, Elsevier Ltd, 2021, https://doi.org/10.1016/j.measen.2021.100202.
[29] L.G. Pittaway, Electron trajectories in ionization gauges, J. Phys. D Appl. Phys. 3 (1970) 1113. http://iopscience.iop.org/0022-3727/3/7/316.
[30] S. Suginuma, M. Hirata, Dependence of sensitivity coefficient of a nude-type Bayard-Alpert gauge on the diameter of an envelope, Vacuum 53 (1999) 177–180.
[31] D.G. Bills, Causes of nonstability and nonreproducibility in widely used Bayard–Alpert ionization gauges, J. Vac. Sci. Technol. A: Vacuum, Surfaces, and Films 12 (1994) 574–579, https://doi.org/10.1116/1.578836.
[32] A. Klopfer, An ionization gauge for measurement of ultra-high vacuum, in: Trans. 8th Nat. Vacuum Symp, 1961, pp. 439–442.
[33] A.Ll Hughes, V. Rojansky, On the analysis of electronic velocities by electrostatic means, Phys. Rev. 34 (1929) 284–290, https://doi.org/10.1103/PhysRev.34.284.
[34] P.C. Arnold, D.G. Bills, M.D. Borenstein, S.C. Borichevsky, Stable and reproducible Bayard-Alpert ionisation gauge, J. Vac. Sci. Technol. 12 (1994) 580–586.
[35] R.T. Bayard, D. Alpert, Extension of the low pressure range of the ionization gauge, Rev. Sci. Instrum. 21 (1950) 571–572, https://doi.org/10.1063/1.1745653.
[36] U. Harten, G. Grosse, W. Jitschin, H. Gentsch, Surface effects on the stability of hot cathode ionization gauges, Vacuum 38 (1988) 167–169, https://doi.org/10.1016/0042-207X(88)90173-X.
[37] I. Figueiredo, N. Bundaleski, O.M.N.D. Teodoro, K. Jousten, C. Illgen, Influence of ion induced secondary electron emission on the stability of ionisation vacuum gauges, Vacuum 184 (2021), https://doi.org/10.1016/j.vacuum.2020.109907.
[38] F. Watanabe, New x-ray limit measurements for extractor gauges, J. Vac. Sci. Technol. A: Vacuum, Surfaces, and Films 9 (1991) 2744–2746, https://doi.org/10.1116/1.577192.
[39] W. Hwang, Y.K. Kim, M.E. Rudd, New model for electron-impact ionization cross sections of molecules, J. Chem. Phys. 104 (1996) 2956–2966, https://doi.org/10.1063/1.471116.
[40] D. Drouin, A.R. Couture, D. Joly, X. Tastet, V. Aimez, R. Gauvin, CASINO V2.42 - a fast and easy-to-use modeling tool for scanning electron microscopy and microanalysis users, Scanning 29 (2007) 92–101, https://doi.org/10.1002/sca.20000.
[41] J. Wagner, W. Stummer, M. Völkerer, A. Hanke, J. Wernisch, Measuring the angular dependent energy distribution of backscattered electrons at variable geometry, Scanning 27 (2005) 298–304, https://doi.org/10.1002/sca.4950270605.
[42] F. Watanabe, Sensitivity reduction and restoration in an extractor gauge, Vacuum 47 (1996) 567–569, https://doi.org/10.1016/0042-207X(96)00021-8.
[43] H. Seiler, Secondary electron emission in the scanning electron microscope, J. Appl. Phys. 54 (1983), https://doi.org/10.1063/1.332840. R1–R18.
[44] S. Fliigge, H. Haken, J. Hamilton, W. Paul, J.O. Treusch, Springer Tracts in Modern Physics - Particle Induced Electron Emission II, 1992. Chapter III.
[45] NIST, Electron-impact cross sections for ionization and excitation, n.d. https://physics.nist.gov/PhysRefData/Ionization/molTable.html. (Accessed 16 March 2022).